Pure Appl. Chem., Vol. 72, Nos. 1–2, pp. 309–315, 2000.

Multiply coated microspheres. A platform for realizing fields-induced structural transition and photonic bandgap*

Ping Sheng †, Weijia Wen, Ning Wang, Hongru Ma, Zhifang Lin, W. Y. Zhang, X. Y. Lei, Z. L. Wang, D. G. Zheng, Wing Yim Tam, and C. T. Chan

Department of Physics, Hong Kong University of Science and Technology, Clear Water Bay, Kowloon, Hong Kong, China

Abstract: Under crossed electric and magnetic fields, multiply coated microspheres form columnar crystallites with an internal structure that transforms from body-centered-tetragonal to face-centered-cubic as the ratio between the magnetic and the electric fields exceeds a minimum value. The observed transition scenario is in excellent agreement with calculations. These multiply coated microspheres also serve as building blocks for photonic crystals. Robust photonic gaps exist in any periodic structure built from such spheres when the filling ratio of the spheres exceeds a threshold.

The electro-rheological (ER) or magneto-rheological (MR) fluids are particle suspensions where the particles have large electric polarizability or magnetic permeability/magnetic moments. The ER or MR effects can order suspended particles into body-centered-tetragonal (bct) mesocrystallites [1–5]. Here, we demonstrate that crossed electric and magnetic fields can induce a martensitic-like transition from the bct to the face-centered-cubic (fcc) structure in mesocrystallites consisting of multiply coated spheres. The multiple coatings serve to enhance the ER and MR effect, and the spheres are referred to as EMR spheres. The cross-sectional scanning electron microscope (SEM) pictures of the EMR spheres are shown in Fig. 1. The cores are uniform glass spheres with diameters of 34 ± 2 μm onto which we coat Ni (approximately 2 μm) using electroless plating technique [6]. A layer of PZT was coated on top of the Ni layer by using the sol-gel method [7]. We have further coated another layer of Ni, followed by a layer of TiO_2. The outer coatings were intended to give a large ER response [8].

In our experiment, we mix the EMR spheres with silicon oil, and put the sample in a cell with four electrodes. The high electric field, at 50 Hz and up to 2 kV/mm, was applied across the top and bottom electrodes, separated 3 mm apart. Another two parallel plates were mounted on two sides, 6 mm apart, and connected to a HP4282A LCR meter. The whole cell was placed in the central region of an electro-magnet (GNW Magnet System, model 3470) with a pole surface diameter of 40 mm and a gap of 20 mm.

The fields-induced transitions are characterized by both in situ measurements and cross-section analysis. At fixed electric field, the structural changes induced by the magnetic field inside the mesocrystallites were monitored by measuring the small dielectric constant changes in a direction perpendicular to both the electric and magnetic fields. The results are summarized in Fig. 2 for a sample with 20% solid volume fraction, at four values of the electric field. The dielectric constant at the small magnetic field region was flat and reversible. For the curve with 2 kV/mm, this region occurred for

Pure Appl. Chem.* **72, 1–331 (2000). An issue of reviews and research papers based on lectures presented at the 1st IUPAC Workshop on Advanced Materials (WAM1), Hong Kong, July 1999, on the theme of nanostructured systems.
†Corresponding author: E-mail: phsheng@ust.hk; Fax: 852-23581652

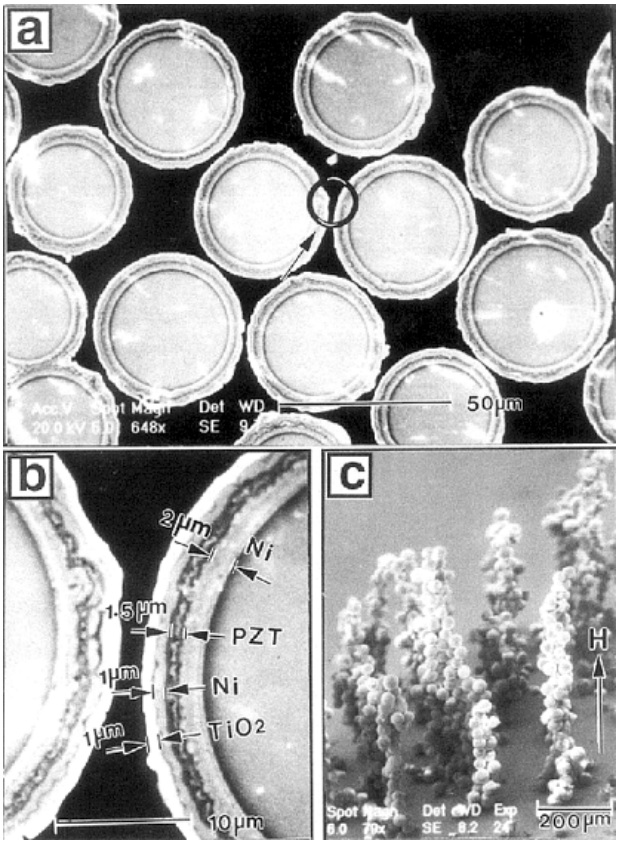

Fig. 1 (a) A cross-sectional SEM picture of the coated spheres. Deviation of the spheres' centers from the cutting plane is the cause for the apparent size variations. The arrow points to a circular region detailed in (b) a SEM cross-sectional picture showing detailed thickness of the four coatings on two adjacent EMR spheres. From the inside out, there is first a 2-μm layer of Ni, followed by 1.5 μm of PZT, then another 1-μm layer of Ni and finally a 1-μm layer of TiO_2. (c) The coated EMR spheres under the influence of a small magnetic stirrer.

magnetic fields less than 30 G. Irreversibility sets in at magnetic fields greater than this value. The associated structural changes inside the columns were monitored by taking many cross-sectional micrograph pictures at various magnetic field values. This is achieved by freezing the configurations in solid epoxy, and cutting the resulting samples. Four such micrograph pictures are shown in Fig. 3, with an applied electric field of 2 kV/mm. Figures 3a and 3b are for the configuration under zero magnetic field, and Figures 3c and 3d are for the configuration at 54 G of applied magnetic field. Other cuttings were taken at 20 G, 30 G, 35 G, 38 G, 40 G, and 50 G. Together with the dielectric constant measurements, they gave the following picture of the bct–fcc transition. At magnetic fields less than 30 G, only the bct structure was seen. From 30 to 50 G, there was a coexistence of local bct structures with local non-bct structures. This coincides approximately with the onset of irreversibility in the dielectric constant measurement. At 54 G, where Figs. 3c and 3d were taken, only the fcc structure was seen. The structural transformation occurred via a cooperative movement of the spheres without any long-range diffusion of the spheres. As such, it can be regarded as a martensitic transition driven by competing external fields.

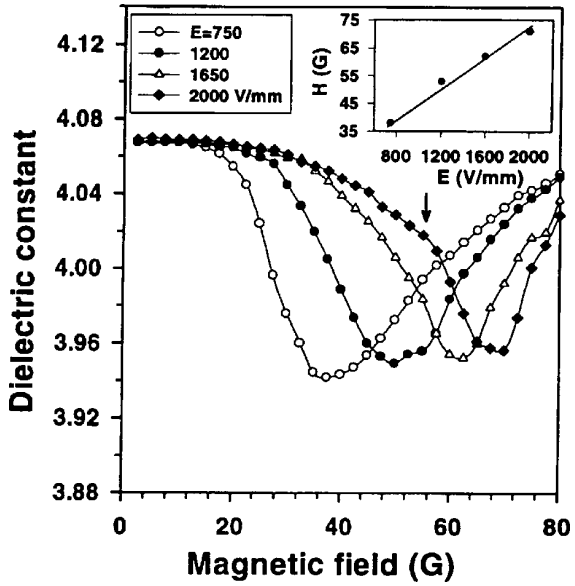

Fig. 2 The sample dielectric constant measured along the *y*-direction (perpendicular to both the electric and magnetic fields) as a function of applied magnetic field, under four different fixed electric fields along the *z*-direction. The dielectric constant is seen to exhibit a 3% dip. The position of the minimum is a linear function of the applied electric field, shown in the upper right inset. The solid volume fraction of the sample is 20%. The arrow indicates the magnetic field value where the fcc structure was observed.

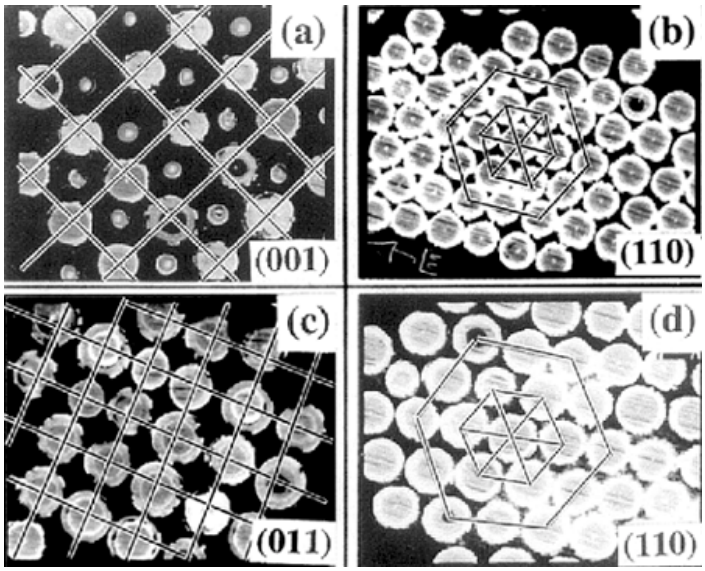

Fig. 3 Cross-sectional SEM pictures of mesocrystallites, with the *E* field along the *z*-direction and *x* is the magnetic field direction, (a) is a cross-section of the (001) plane and (b) is a cross section of the (110) plane for a sample frozen (in epoxy) at $E = 2$ kV/mm with zero magnetic field. The nearly square lattice (with a displaced sphere at the center of each square) along the (001) plane and a hexagonal lattice along the (110) plane are the signatures of a bct lattice. For a sample frozen (in epoxy) at $E = 2$ kV/mm and $H = 54$ G, (c) is a cross section of the (011) plane (the fcc{100}) and (d) is a cross section of the (110) plane (the fcc{111}). Taken together, (c) and (d) give direct evidence to a fcc lattice.

The physics underlying such a structural transition is elucidated by calculating the free energy of the EMR system under external fields. In our calculations, we assume that the spheres form columns, as observed experimentally. We consider the free energy density of the EMR fluid, F = F_E + F_H, where F_E and F_H are the electrostatic and magnetostatic part of the free energy respectively. The electrostatic free energy density is given by $F_E = -\bar{\varepsilon}_{zz}E^2/8\pi$. Here, *z* is the direction of the electric field *E*, and $\bar{\varepsilon}_{zz}$ is the *zz* component of the effective dielectric tensor for the anisotropic composite system. The effective dielectric constant ε_{zz} of the mesocrystal inside the columns is calculated through the Bergman–Milton representation [5,9]: The overall $\bar{\varepsilon}_{zz}$ can then be found from $\bar{\varepsilon}_{ZZ} = f_c\,\varepsilon_{zz} + (1-f_c)\,\varepsilon_2$. The magnetic free energy density is given by

$$F_H = F_m - \vec{M}\bullet\vec{H} + 2\pi\eta_{\alpha\beta}M_\alpha M_\beta \tag{1}$$

The first term

$$F_m = -\frac{1}{2\Omega}\sum_i \vec{m}_i \bullet \sum_{j\neq i}\frac{1}{r_{ij}^3}\left[3\hat{n}(\hat{n}\bullet\vec{m}_j) - \vec{m}_j\right] \tag{2}$$

is the dipole–dipole interaction due to the permanent moments of the EMR spheres. The second term is the interaction with the applied magnetic field $\vec{H}$ and the magnetization of the entire system $\vec{M}$. The third term takes care of the depolarization effects, where $\eta_{\alpha\beta}$ are the demagnetization factors. A spin dynamics simulation is used to determine the orientation of $\vec{m}_i$ (magnitude fixed at 1.0×10^{-6} emu) and hence F_m and $\vec{M}$. We describe our system by a body-centered-orthorhombic unit cell, which contains bct and fcc structures as special cases. We align the *c* axis with the *E* field and the *a* axis with the *H* field. We found that up to *H* = 60 G, the minimum energy state is associated with *c* = 2*R*. In addition, the spheres must be in physical contact with each other, since there are no repulsive forces other than the hard sphere repulsions. At *H* = *0*, the ground state is found to be the bct structure, with *a*/*c* = $\sqrt{6}/2$ (and *b* = *a*), as seen experimentally. The closed-packed (110) plane is invariant under the bct → fcc transformation. Together with the constraint of *c* = *2R*, the transformation path can be described by the equation $b^2 = 12R^2 - a^2$. The hard sphere condition ($a \geq 2R$, $b \geq 2R$) requires $1 \leq a/c \leq \sqrt{2}$, with the limits corresponding to fcc structures oriented differently with respect to the magnetic field. We performed

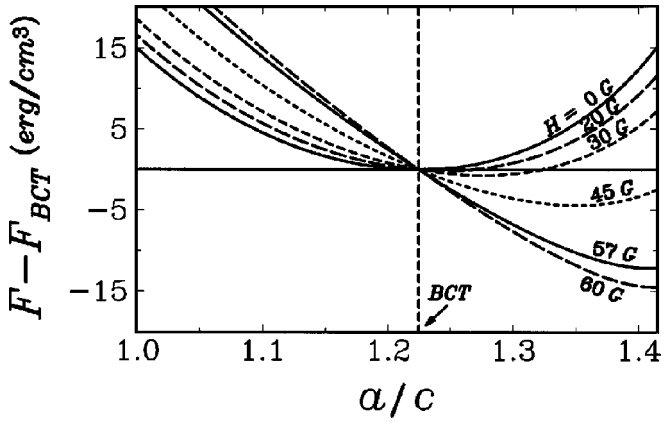

Fig. 4 Calculated sum of the electrostatic and magnetostatic free energy densities, minimized with respect to the *c* and *b* axes values, are plotted as a function of the *a*/*c* ratio. The energy of the bct structure is used as reference.

energy calculations along this path, and the results are shown in Fig. 4 for different values of magnetic field strengths with a fixed applied electric field of 2 kV/mm. From Fig. 4, we see that for H below ~30 G, bct remains the optimal structure. For magnetic fields above 30 G, the minimum free energy state rapidly moves to the fcc structure. This coincides with the observation of non-bct structures at these magnetic fields. We note that a increases under the action of the H fields implies a decrease of $\bar{\varepsilon}_{yy}$. This is indeed observed in Fig. 2.

When assembled together, these EMR spheres also have novel optical properties. With multiple coatings of variable thicknesses, these coated spheres have continuously tunable scattering cross-sections and resonances for electromagnetic waves. Such unique and tunable optical properties make them viable building blocks for photonic bandgap [10] (PBG) materials. PBG is a spectral gap in the electromagnetic wave spectrum in which light can only exist as evanescent waves, and PBG materials (sometimes called photonic crystals) are materials that exhibit such a gap. The analogue for electrons would be the electronic band gap and semiconductors. However, unlike electronic semiconductors, PBG does not exist in nature and has to be fabricated. Although rapid advances have been made in the past decade [11], making 3D PBG material at IR or optical frequencies remains a challenge, and we are going to argue that these coated spheres are viable alternatives to the existing PBG material. The systems have the added advantage that the crystal structure can be changed by external fields.

We will first show by explicit calculations that any structure built from these spheres possesses PBG. The calculations are based on the multiple scattering technique (MST) [12]. We consider a generic system where the building blocks are touching metallo-dielectric spheres. The spheres have metallic cores coated with a dielectric coating ($\varepsilon = 12$ and thickness ~5% of the radius). The metal is modelled by $\varepsilon = -200$. In Fig. 5, we show that essentially any periodic structure constructed from these spheres have photonic bandgaps. We show in the figure the frequency (marked by the squares) and the size (marked by the bars) of the photonic gaps for a variety of structures. The angular frequency (ω) in

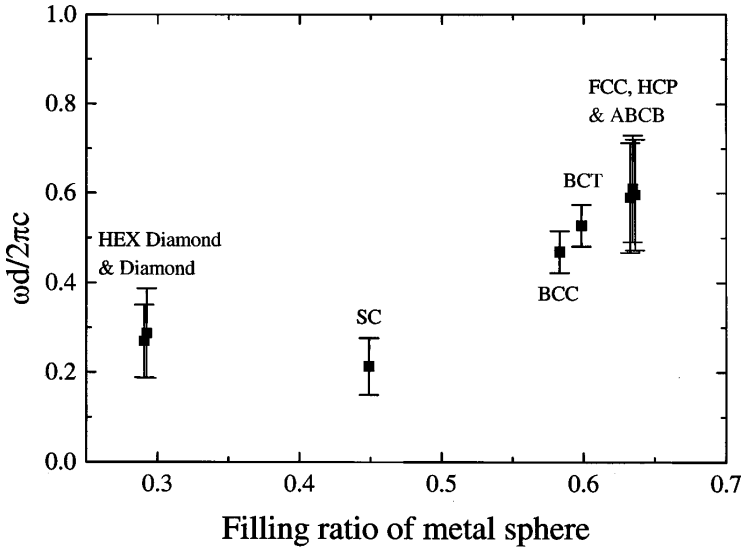

Fig. 5 The photonic bandgaps for different crystal structures. All structures are made of touching metallo-dielectric spheres with a 5%-radius dielectric coating $\varepsilon = 12$. The filling ratio is that of the metallic core. HEX diamond, bct and ABCB refers to hexagonal diamond, body-centered-tetragonal, and a close-packing polytype of with planes stacked in a repeated ABCB sequence, respectively. Other symbols such as fcc have their usual meaning. d denotes the diameter of sphere.

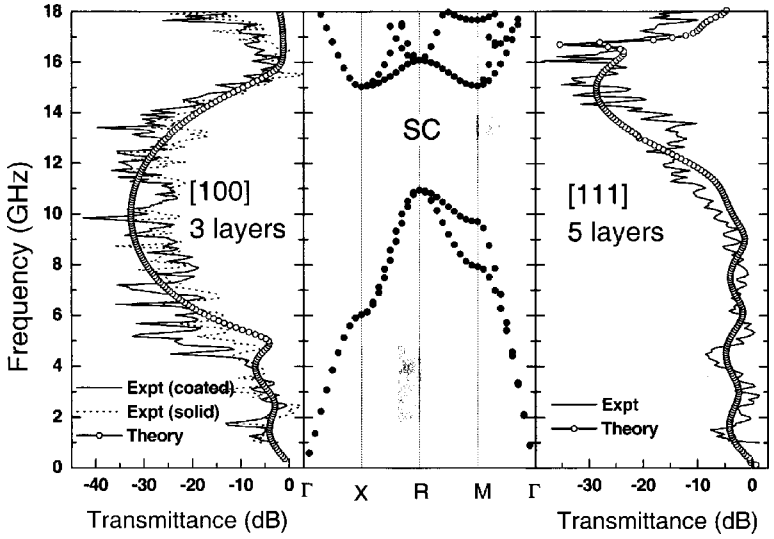

Fig. 6 Comparison of the calculated photonic band structure (middle panel) for a simple cubic photonic crystal with measured and calculated transmittance through a 3-layer (100) orientated slab (left panel) and a 5-layer (111) slab (right panel). The solid lines in the left and right panels are the transmittance for metal-coated spheres, while the dotted lines are for solid metal spheres. Calculated transmittances are given as open circles. See text for details.

the figure is scaled by $2\pi c/d$ where d is the diameter of the spheres. We found that an absolute photonic gap always emerges for such a system when the volume filling ratio of the metallic spheres exceeds a threshold, and the size of the gap increases monotonically as a function of the filling ratio. Such behavior holds for all the structures we have considered. A potentially useful property of the present system is that the size and frequency of the photonic gap depend on the filling ratio and the short-range order rather than on symmetry and long-range order. This can be deduced from Fig. 5. Note that both the diamond and the hexagonal diamond structure have the same 4-fold coordination and local order, but different symmetries. The photonic gap has almost the same size and frequency. The same is true for the fcc and hcp structures, which have the same local coordination but a different stacking sequence of close-packed planes. Even an ABCB stacking of close-packed planes has essentially the same absolute gap. We note that these coated sphere-based PBG crystals are different from conventional dielectric PBG crystals in which symmetry and long-range order are of prime importance.

We have constructed photonic crystal slabs and measured the transmittance in the microwave regime. Simple cubic slabs are constructed with spheres that are 12.7 mm in diameter. The lattice constant a = 13.4 mm so that the spheres occupy 45% of the volume in the crystal. In Fig. 6, we compare the calculated photonic bandgap for the simple cubic photonic crystal with the transmission spectra through finite-sized slabs in two different directions. The middle panel is the photonic band structure, with metal spheres modeled by $\varepsilon = -10^4$. An absolute gap is observed between 11 and 15 GHz. In the left and right panels, we compare the experimental and calculated transmission spectra. The two experimental spectra in the left panel correspond to the transmission through a 3-layer slab in the (001) direction of two types of spheres: (i) solid metal spheres and (ii) metal-coated spheres that have plastic cores coated with a 40-μm copper coating. We notice that the coated spheres and solid metal spheres give very similar transmission spectra. This is expected since the skin depth for Cu is sub-micron in this regime. The calculated transmission, which agrees well with the measured spectra, corresponds to transmission through solid metal spheres modelled with $\varepsilon = (-10^4 + 10^4 i)$. From the band structure, we see that there

is a directional gap along the ΓX direction from about 6 to 15 GHz. This corresponds well with the calculated and measured transmission spectra, which shows a wide stop band at the same frequency range. The right panel compares the calculated and measured transmission through the (111) direction of a 5-layer slab of the simple cubic structure. There is again good agreement between theory and experiment. The stop band at 14 GHz (skewed towards higher frequencies) is derived from the absolute gap.

In short, we observed external fields-induced martensitic transition in meso-crystallites of multiply coated spheres. The observed transition can be understood in terms of the competition between electric and magnetic energy. In addition, we found that photonic crystals built from the multiply coated spheres have the unique property that any periodic structure of such spheres exhibits photonic gaps. Proof of principle experiments at the microwave frequencies give results that are in good agreement with theory.

ACKNOWLEDGMENTS

We wish to acknowledge the support by HKUST Research Infrastructure Grant No. RI 93/94.SC09, CERG HKUST 6142/97P, HKUST6136/97P and the William Mong Solid State Cluster Laboratory.

REFERENCES

1. R. Tao and J. M. Sun. *Phys. Rev. Lett.* **67** (1991) 398; R. Tao and J. M. Sun. *Phys. Rev. A* **44,** R6181 (1991).
2. G. Bossis, H. Clercx, Y. Grasselli, E. Lemaice. In *Electrorheological Fluids*, R. Tao and G. D. Roy, eds., p.153, World Scientific (1994); H. Clercx and Bossis. *Phys. Rev*. *E* **48,** 2721 (1993).
3. L. C. Davis. *Phys. Rev. A* **46,** R719 (1992).
4. R. Friedberg and Y. K. Yu. *Phys. Rev. B* **46,** 6582 (1992).
5. H. Ma, W. Wen, W. Y. Tam, P. Sheng. *Phys. Rev. Lett.* **77,** 2499 (1996).
6. J. W. Severin, R. Hokke, H. Venderwel, G. deWith. *J. Electrochem. Soc.* **140**, 682 (1983).
7. C. J. Briker and G. W. Scherer. *Sol-Gel Science: The Physics and Chemistry of Sol-Gel Processing*, Academic Press, New York (1990).
8. W. Y. Tam, G. H. Yi, W. Wen, H. Ma, M. M. T. Loy, P. Sheng. *Phys. Rev. Lett.* **78**, 2987 (1997).
9. D. J. Bergman, *Phys. Rep.* **43** 377 (1978); D. J. Bergman. *Phys. Rev. B* **19**, 2359 (1979); G. W. Milton, *Appl. Phys. A* **26**, 1207 (1981); G. W. Milton. *J. Appl. Phys.* **52**, 5286 (1980).
10. E.Yablonovitch. *Phys. Rev. Lett.* **58**, 2059 (1987); S. John. *Phys. Rev. Lett.* **58**, 2486 (1987); J. D. Joannopoulos, R. D. Meade, J. Winn. *Photonic Crystals*, Princeton University Press, New York (1995).
11. See, e.g., S. Y. Lin et al. *Nature* **394**, 251 (1998); E. G. Wijnhoven and W. L. Vos. *Science* **281**, 802 (1998).
12. There are many different formulations: See, e.g., K. Ohtaka, *J. Phys. C* **13**, 667 (1980); N. Stefanou, V. Karathanos, and A. Modinos. *J. Phys.* **4**, 7389 (1992); X. D. Wang, X.-G. Zhang, Q. L. Yu, B. N. Harmon. *Phys. Rev. B* **47**, 4161 (1993); G. Tayeb and D. Maystre. *J. Opt. Soc. Am. A* **14**, 3323 (1997); L. M. Li and Z.Q. Zhang. *Phys. Rev. B* **58**, 15589 (1998); N. Stefanou, V. Yannopapas, A. Modinos, *Computer Phys. Commun.* **113**, 49 (1998).